Research Square

Preprints are preliminary reports that have not undergone peer review.
They should not be considered conclusive, used to inform clinical practice,
or referenced by the media as validated information.

Spatiotemporal and progression heterogeneity of Parkinson's disease leveraging multimodal data

Zhining Li
The Second Affiliated Hospital of Soochow University
Pei Lu
Xuzhou Medical University
Hongyu Bi
Xuzhou Medical University
Yumeng Liu
Xuzhou Medical University
Dixia Cong
The Second Affiliated Hospital of Xuzhou Medical University
Can Li
The Second Affiliated Hospital of Xuzhou Medical University
Aiping Gong
The Second Affiliated Hospital of Xuzhou Medical University
Hua Yang
The Second Affiliated Hospital of Xuzhou Medical University
Liangqun Rong
The Second Affiliated Hospital of Xuzhou Medical University
Lishun Xiao
xiaolishun@xzhmu.edu.cn

Xuzhou Medical University

Article

Keywords: Parkinson's disease, Multimodal, Disease progression, Gait analysis, Cognitive decline

Posted Date: March 6th, 2026

DOI: https://doi.org/10.21203/rs.3.rs-8989360/v1

License: This work is licensed under a Creative Commons Attribution 4.0 International License.
Read Full License

Additional Declarations: No competing interests reported.

Spatiotemporal and progression heterogeneity of Parkinson's disease leveraging multimodal data

Zhining Li[1, *], Pei Lu[2, *], Hongyu Bi[2], Yumeng Liu[2], Dixia Cong[1], Can Li[1], Aiping Gong[1], Hua Yang[1], Liangqun Rong[1, #], Lishun Xiao[1, #]

1 Department of Neurology, The Second Affiliated Hospital of Xuzhou Medical University, Xuzhou, Jiangsu, 221006, China
2 School of Public Health, Xuzhou Medical University, Xuzhou, Jiangsu, 221004, China

* These authors have contributed equally to this work and share first authorship.
# Corresponding authors: No. 209 Tongshan Road, Xuzhou Medical University, Xuzhou, Jiangsu Province, 221004, China (Lishun Xiao, E-mail: xiaolishun@xzhmu.edu.cn); No. 32 Meijian Road, Xuzhou, Jiangsu Province, 221006, China (Liangqun Rong; E-mail: zningdoctor@126.com).

Abstract

Parkinson's disease (PD) is a clinically and biologically heterogeneous neurodegenerative disorder with divergent progression trajectories. Conventional longitudinal cohorts often lack the temporal resolution required for comprehensive disease progression modeling. This study leverages multimodal biomarkers to systematically identify and characterize interpretable PD subtypes with distinct temporal progression patterns. A cohort of 147 participants (107 PD, 40 healthy controls) underwent comprehensive multimodal assessments, including clinical evaluations, quantitative gait analysis, and neuroimaging. Biomarkers demonstrating monotonic associations with disease progression and significant group differences were selected, adjusted for covariates, and normalized. The subtype and stage inference (SuStaIn) model was applied to delineate progression subtypes, which were externally validated. Analysis revealed three reproducible PD subtypes: gait-predominant, intermediate motor, and cognitive-predominant, each defined by unique progression trajectories. Subtype classification exhibited high confidence and generalizability. The gait-predominant subtype showed early impairments in step length, gait speed, and turning, with late cognitive decline. The intermediate motor subtype featured early deterioration in axial and appendicular metrics alongside intermediate structural changes. The cognitive-predominant subtype displayed early cerebellar/brainstem involvement, rapid cognitive decline, and severe multimodal deficits, reflecting a malignant phenotype with the highest disease burden. These findings demonstrate biologically grounded divergence in PD progression, offering a scalable framework for individualized staging, mechanistic stratification, and precision-medicine trial design.

Keywords: Parkinson's disease; Multimodal; Disease progression; Gait analysis; Cognitive decline

1 Introduction

Parkinson's disease (PD), the second most prevalent neurodegenerative disorder, is marked by the selective degeneration of dopaminergic neurons in the substantia nigra and the progressive, pathological accumulation of misfolded α-synuclein aggregates in multiple brain regions[1]. The clinical manifestations of PD encompass both motor symptoms (e.g., tremor, rigidity, bradykinesia, and postural instability) and non-motor symptoms (e.g., emotional disturbances, autonomic dysfunction, and cognitive impairment)[2]. Patients follow divergent trajectories across motor dysfunction, gait disturbance, cognitive decline, and regionally specific neurodegeneration, suggesting the presence of distinct clinical subtypes rather than a single disease pathway[3]. Emerging evidence highlights substantial clinical, biomarker, and imaging heterogeneity among PD patients. The clinical heterogeneity poses a formidable challenge for prognosis, biomarker development, and precision therapeutics[4]. To address this variability, researchers increasingly employ data-driven clustering approaches integrating multimodal data, such as clinical assessments, scale-based evaluations, imaging data, and biomarker profiles[5–8]. Comprehensive research for PD necessitates the integration of multimodal data as unimodal snapshots fail to account for the interplay between biology, clinical symptom, and disease evolution. However, most existing studies on PD heterogeneity predominantly remained static, limiting their capacity to comprehensively capture the dynamic progression of clinical symptoms, as certain key indicators may evolve over time[5,6,8–10].

Understanding PD heterogeneity in progression has relied largely on longitudinal cohort studies, which provide direct temporal information but are constrained by long and irregular follow-up intervals, attrition, and incomplete coverage of the disease course[11,12]. These limitations reduce the temporal resolution and generalizability of inferred trajectories and make it challenging to reconstruct full disease courses from limited serial observations. As a complementary strategy, wearable and remote monitoring can densely capture motor and gait features in naturalistic settings, but integrating such multimodal data into coherent progression models remains nontrivial[13–15]. To overcome these limitations, disease-progression modeling has emerged as a powerful framework for inferring latent temporal structure from cross-sectional data[16]. The event-based model offered a probabilistic approach to estimate sequences of indicator abnormality without longitudinal follow-up, and later refinements such as the discriminative event-based model improved robustness and scalability across heterogeneous indicator sets[17,18]. However, these models assume a single global progression sequence and thus cannot capture the diversity characteristic of PD.

The subtype and stage inference (SuStaIn) framework was developed to address this limitation by simultaneously identifying distinct progression patterns and estimating subtype-specific disease stages from cross-sectional indicators[19,20]. Given the extensive heterogeneity and limited longitudinal coverage typical of PD datasets, SuStaIn offers a biologically interpretable and data-efficient approach for mapping disease progression[21,22]. In the present study, we implement the SuStaIn algorithm to elucidate distinct trajectories of clinical symptom progression of PD patients leveraging a multimodal dataset. Our framework synergizes three critical modalities: standardized clinical assessments (capturing the disease burden), high-precision quantitative gait metrics (providing granular motor control phenotyping), and neuroimaging biomarkers (revealing underlying structural degeneration). This tripartite approach addresses a key limitation in PD research, which is the frequent dissociation between observable functional decline and neural pathology, by establishing quantifiable links between microscale neural changes and macro-scale clinical manifestations. Through SuStaIn's probabilistic modeling, we identify reproducible PD subtypes characterized by their progression sequences, with particular emphasis on differentiating motor-dominant from rapidly progressing cognitive-motor phenotypes. The gait biomarkers' inclusion proves particularly transformative, detecting subtle but clinically meaningful motor signatures that conventional Movement Disorder Society-Unified PD rating scale (MDS-UPDRS) evaluations often overlook.

2 Materials and methods

2.1 Participants

All participants were recruited from the Department of Neurology at the Second Affiliated Hospital of Xuzhou Medical University, Xuzhou, China, between March 2023 and June 2025. The inclusion criteria for PD patients were: (i) *De novo* treatment-naive patients through the diagnostic criteria of the International Parkinson's Disease and Movement Disorders Society 2015[23]; (ii) Patients or their families signed the informed consent form. The exclusion criteria for PD patients were: (i) Patients with severe mental disorders or severe cognitive impairment who cannot cooperate in completing the study questionnaire and assessment; (ii) Patients with coinfections, or severe chronic or acute diseases (e.g., tumors, severe organ insufficiency, etc.); (iii) Patients who have undergone brain surgery or deep brain electrical stimulation surgery for other reasons before. The inclusion criteria for healthy controls (HCs) were: (i) Individuals without severe chronic or acute diseases; (ii) Individuals who have not undergone brain surgery or deep brain electrical stimulation surgery before; (iii) Individuals who signed the informed consent form. Finally, this study enrolled a total of

147 participants, comprising 107 individuals with PD and 40 HCs (see Figure 1 for an overview of the study protocol).

This study was approved by the Ethics Committee of Xuzhou Medical University (XZHMU-25Z7069) and conducted in accordance with the *Declaration of Helsinki*. Written informed consent was obtained from all participants.

2.2 Data acquisition and processing

Demographic data were collected from all participants. For the PD cohort, disease duration was recorded as the time elapsed since motor symptom onset. Comprehensive clinical assessments were performed to evaluate disease severity and multidimensional symptoms. The MDS-UPDRS and Hoehn & Yahr (H-Y) stage were assessed by trained neurologists to quantify motor severity and global disease burden. Additionally, standardized questionnaires were collected to assess specific symptom domains: the eating assessment tool (EAT-10) for bulbar dysfunction and dysphagia risk, the 9-item wearing-off questionnaire (WOQ-9) for motor complications, the 39-item PD questionnaire (PDQ-39) for health-related quality of life, and the non-motor symptoms questionnaire (NMSQ) for non-motor symptom load.

A multimodal data acquisition protocol was implemented for all participants, encompassing clinical assessments, neuroimaging, and wearable sensor-based quantitative gait analysis. Global cognitive function was assessed using the mini-mental state examination (MMSE). All participants underwent structural brain imaging using a 1.5T GE OPTIMA MR360 system (General Electric Company, USA). Detailed acquisition parameters are provided in the Supplementary methods. The T1-weighted magnetic resonance imaging (MRI) scans were processed using the FreeSurfer image analysis suite (version 7.4.1, http://surfer.nmr.mgh.harvard.edu) to perform cortical reconstruction and volumetric segmentation[24]. The automated processing pipeline included several key steps: motion correction, removal of non-brain tissue via a hybrid watershed/surface deformation algorithm, automated Talairach transformation, and segmentation of subcortical white matter and deep grey matter structures[25]. Detailed steps for image processing are provided in the Supplementary methods. Gait characteristics were quantified using a custom wireless inertial measurement unit (IMU) system (Gyenno)[26]. Ten IMU sensors, each comprising tri-axial accelerometers and gyroscopes sampled at 100 Hz, were securely attached to ten body locations, including bilateral wrists, chest, lower back, thighs, shanks, and shoe dorsum, to capture full-body kinematic trajectories during ambulation. All sensors were synchronized via Bluetooth low energy prior to data

acquisition. Participants performed motor tasks according to the standardized Ruiping assessment protocol, with no spatial constraints imposed on movement. The raw IMU data were processed to extract a comprehensive set of gait parameters[27], including but not limited to joint angular kinematics, velocity, cadence, step length, and the relative durations of stance and swing phases. This approach enabled a quantitative analysis of each participant's functional walking performance.

Finally, the covariates, clinical assessments, T1-weighted structural MRI data and quantitative gait data were collected. Indicators (or features) with a missing rate exceeding 30% were excluded, otherwise were imputed using the median. Common assessments shared by both the PD and HC cohorts included structural MRI, quantitative gait analysis, and MMSE.

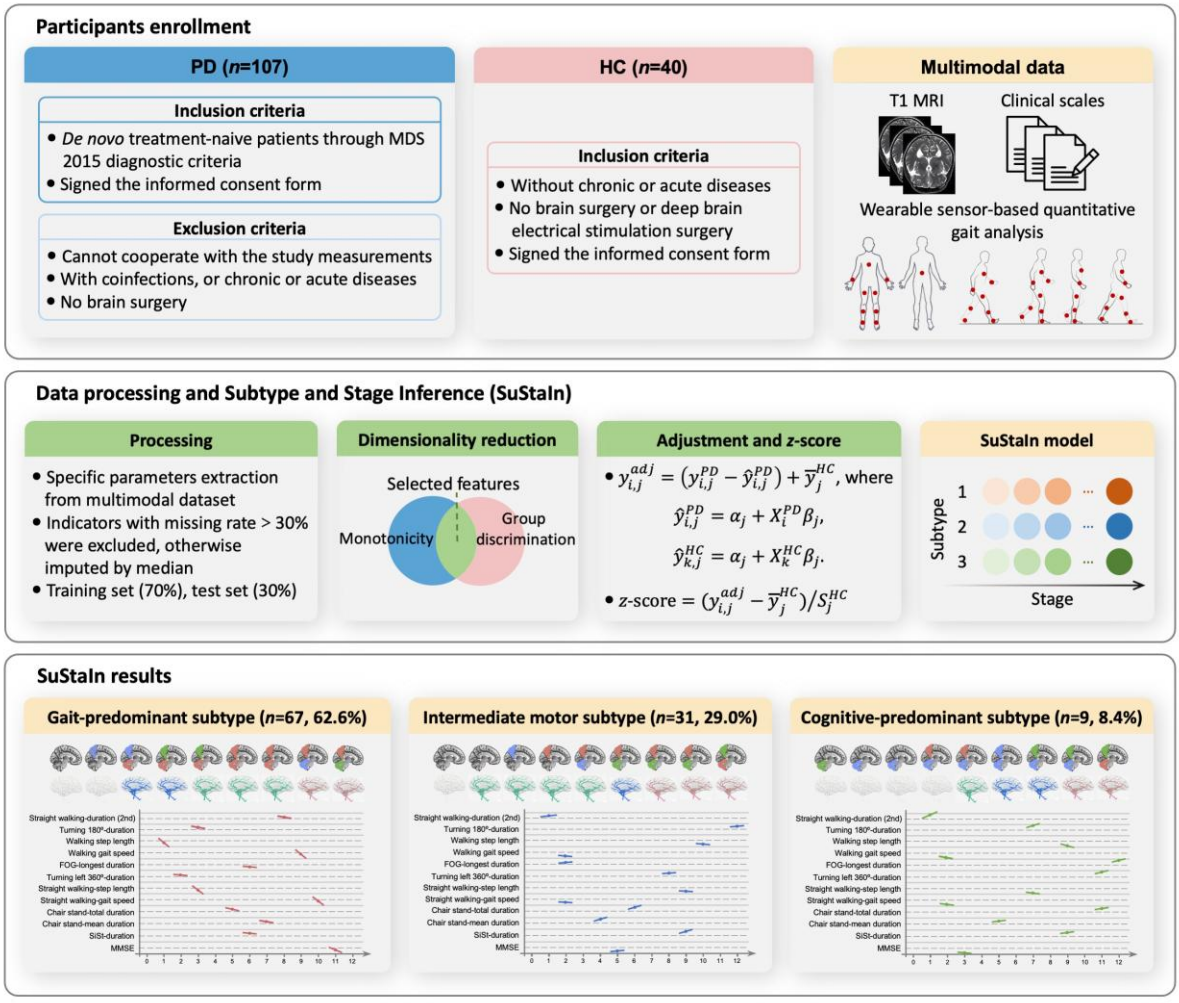


Figure 1 Study workflow illustrating participant enrollment, data processing, and modeling results

2.3 Subtype and stage inference modeling

The SuStaIn algorithm was adopted to unravel the underlying heterogeneity of disease progression in PD[20,28–30]. SuStaIn reconstructs pseudo-longitudinal progression trajectories from cross-sectional data by

identifying distinct patterns of abnormality accumulation. The method probabilistically infers disease subtypes, each characterized by a unique sequence of indicator changes over time, and assigns each participant a subtype group probability alongside a continuous disease stage estimation along the corresponding trajectory. Detailed mathematical description and algorithmic overview of the SuStaIn framework are provided in the Supplementary methods.

The dataset was partitioned into a training set (70%) and a test set (30%) prior to any modeling procedures. Considering the computationally intensive nature of SuStaIn, we developed a multistage, data-driven dimensionality reduction pipeline for multimodal indicators selection in the training set. Our approach prioritized indicators demonstrating pathological specificity, temporal progression dynamics, and group discriminability between PD and HC cohorts. The selection protocol comprised two steps: (i) Monotonic progression validation: Indicators in the PD cohort were assessed for monotonic relationships by Spearman's correlation with disease duration, retaining the ones only demonstrating significant temporal progression patterns. (ii) Group discrimination: Indicators without significant differences between-group by t-test were excluded, establishing pathological relevance through HC-PD discriminability[17].

Given that covariates may influence the multimodal biomarkers, adjustment of PD patients' indicators is necessary especially when there exist significant differences for covariates between HC and PD cohorts[31,32]. Let $y_{i,j}^{PD}$ and $y_{i,j}^{adj}$ denote the original and adjusted value of the jth biomarker for the ith PD patient, respectively. And the adjustment formula is given by $y_{i,j}^{adj} = \left(y_{i,j}^{PD} - \hat{y}_{i,j}^{PD}\right) + \overline{y}_j^{HC}$, where $\overline{y}_j^{HC}$ represents the mean of the jth biomarker in the HC group, and $\hat{y}_{i,j}^{PD} = \alpha_j + X_i^{PD}\beta_j$ with X_i^{PD} being the vector of covariates for the ith PD patient. The coefficients α_j and β_j are derived from the regression equation $\hat{y}_{k,j}^{HC} = \alpha_j + X_k^{HC}\beta_j$, where $\hat{y}_{k,j}^{HC}$ and X_k^{HC} are the expected value of the jth biomarker and the covariates vector for the kth HC. Subsequently, all adjusted biomarkers of PD cohort are standardized to z-scores relative to the HC cohort, i.e., $(y_{i,j}^{adj} - \overline{y}_j^{HC})/S_j^{HC}$, where S_j^{HC} represents the standard deviation of the jth biomarker in HC cohort. This transformation quantifies the deviation of each biomarker for PD patients from HC in units of standard deviation. Directional consistency in progression modeling, which is essential for the SuStaIn algorithm as it requires higher values to indicate greater pathology, is ensured by inverting the z-scores of biomarkers that naturally decrease with disease progression (e.g., gait speed, step length, MMSE score, and neuroanatomical volumes or thicknesses) through multiplication by -1.

SuStaIn model fitting was performed using the piecewise linear *z*-score framework, in which biomarker progression is represented as discrete transitions across increasing severity thresholds. Hyperparameters, threshold definitions, initialization strategy, and Markov Chain Monte Carlo uncertainty quantification are provided in Supplementary methods. The determination of the number of subtypes was conducted exclusively on the training set, with model selection guided by 10-fold cross-validation using the cross-validation information criterion (CVIC). CVIC serves as a rigorous model selection metric that penalizes complexity to mitigate overfitting; a lower value indicates a better balance between model fit and parsimony[33]. Model stability was assessed through 10-fold cross-validation on the training set, with consistency of event sequences across folds confirming robustness against partition artifacts. For external validation, we applied covariate adjustment and *z*-score standardization parameters derived from training-set HCs to the test set. The final SuStaIn model, with fixed number and event sequences from training, was then deployed for test-set subtype and stage assignment. Comparative analysis of subtype distributions and characteristics between training and test sets provided direct evidence of external validity and clinical applicability.

To delineate the distinct pathological signatures associated with each subtype, comprehensive analyses were performed across each data modality. Gait parameters were systematically categorized into functional domains (e.g., pace, rhythm, turning, stability) and aggregated into composite scores for each domain to facilitate cross-subtype profile comparisons. Furthermore, subtype-specific correlation analyses were conducted to assess the relationship between MMSE scores and regional neuroimaging biomarkers. To substantiate the clinical relevance of the data-driven disease stages, Spearman's correlation analysis was employed to evaluate the monotonic association between each patient's assigned SuStaIn stage and established clinical severity metrics, including disease duration and MMSE scores. We also performed an exhaustive post-hoc analysis employing 6 independent clinical scales, including H-Y stage, MDS-UPDRS, EAT-10, WOQ-9, PDQ-39, NMSQ. To elucidate the alignment between data-driven disease progression trajectories and conventional clinical staging, Spearman's correlation analysis was conducted to evaluate the relationship between the continuous SuStaIn stages and ordinal H-Y stages, both across the entire cohort and within individual subtypes.

2.4 Statistical analysis

Categorical variables were expressed as frequencies and percentages (*n*, %), with between-group

differences were assessed by Chi-squared test. Continuous variables were initially evaluated for normality using Shapiro-Wilk's test and for homogeneity of variance using Levene's test. Normally distributed variables were reported as mean±standard deviation and analyzed using t-test (for two-group comparisons) or one-way analysis of variance (for multi-group comparisons). Non-normally distributed variables were presented as median [P_{25}, P_{75}] and analyzed using Kruskal-Wallis' test. Post-hoc analyses were conducted with Tukey's test for normal variables and Mann-Whitney U test with Bonferroni's correction for non-normal variables. A two-sided *P* value threshold of 0.05 was established for statistical significance. All statistical analyses were performed using Python (version 3.7) with the SciPy, statsmodels, and scikit-learn libraries.

3 Results

3.1 Participant characteristics

Following the aforementioned dimensionality reduction protocol, we identified a final set of 16 multimodal biomarkers that exhibited both significant dynamic progression and pathological relevance. This optimal feature set comprised 11 quantitative gait metrics (capturing gait pace, turning, stability, and chair-stand performance), 1 clinical assessment, i.e., global cognitive measure (MMSE), and 4 neuroimaging MRI markers (brainstem volume, left cerebellar white matter, right vessel volume, and right subparietal thickness), collectively capturing multifaceted aspects of PD progression suitable for stage-based modeling. A comprehensive list of all candidate indicators, along with detailed statistical metrics for the selection process, is provided in Supplementary Table S1. The selected biomarkers and covariates, including gender, age, height, thigh length, calf length, and estimated total intracranial volume (eTIV) are summarized in Table 1. The PD cohort in the training set was significantly older than HCs (P=0.001), and exhibited shorter thigh lengths. Notably, the PD cohort demonstrated pronounced motor and cognitive impairment, characterized by prolonged gait and turning durations, reduced step length and gait speed, and lower MMSE scores (all P<0.05).

Table 1 Demographic, clinical, gait, and neuroimaging characteristics of HC and PD cohorts in training set

Characteristics	HC (n=28)	PD (n=74)	$t/\chi^2/U$	P	P for r
Covariates					
Gender: Male	19 (47.50)	60 (56.10)	0.55	0.458	-
Age	62.00 [55.00, 70.25]	70.00 [64.00, 75.00]	1347.00	**0.001**	-
Height (cm)	164.40±7.92	164.55±7.35	-0.11	0.917	-
Thigh length (cm)	47.00 [43.50, 49.00]	43.00 [40.00, 46.00]	2842.50	**0.004**	-
Calf length (cm)	45.00 [42.75, 48.00]	43.00 [41.00, 45.00]	2700.50	0.067	-
eTIV	1284747.45 [1214595.72, 1408208.08]	1335937.12 [1202481.04, 1450566.09]	1949.00	0.089	-
Wearable sensor-based gait metrics					

Straight walking-duration (2nd)(s)	3.48 [2.94, 4.38]	4.43 [3.21, 6.09]	1352.00	**0.003**	**0.037**
Turning 180°-duration (s)	1.87 [1.60, 2.22]	3.01 [2.19, 4.30]	686.00	**<0.001**	**0.032**
Walking step length (cm)	52.87 [43.48, 56.86]	40.97 [30.13, 49.65]	2846.00	**<0.001**	**0.003**
Walking gait speed (m/s)	0.85±0.22	0.67±0.25	3.93	**<0.001**	**0.031**
FOG-longest duration (s)	0.22±1.39	1.74±4.68	3.02	**0.008**	**0.001**
Turning left 360°-duration (s)	10.41 [8.16, 14.46]	14.35 [11.04, 22.43]	1318.00	**<0.001**	**0.003**
Straight walking-step length (cm)	51.32 [41.43, 56.12]	39.72 [28.13, 50.45]	2889.50	**<0.001**	**0.003**
Straight walking-gait speed (m/s)	0.75±0.24	0.63±0.25	2.56	**0.011**	**0.012**
Chair stand-total duration (s)	4.79 [2.67, 14.16]	18.48 [14.51, 22.93]	705.50	**<0.001**	**0.035**
Chair stand-mean duration (s)	2.91 [2.49, 3.82]	3.85 [2.90, 4.66]	1288.50	**0.005**	**0.019**
SiSt-duration (s)	1.08 [0.95, 1.24]	1.37 [1.10, 1.66]	1059.50	**<0.001**	**0.011**
Clinical assessment					
MMSE	28.00 [26.50, 29.00]	22.00 [19.00, 25.50]	3643.00	**<0.001**	**0.005**
Neuroimaging biomarkers					
Left cerebellum white matter	14087.35 [12085.17, 15402.80]	14100.90 [12798.10, 16202.70]	2051.00	**0.003**	**0.013**
Brain stem	19044.45 [17968.68, 20625.08]	19676.10 [17807.95, 21370.15]	2053.00	**0.001**	**0.046**
Right vessel	7.70 [0.00, 15.05]	0.00 [0.00, 12.70]	2478.50	**0.040**	**0.001**
Right subparietal thickness	2.67 [2.44, 3.01]	2.66 [2.40, 2.88]	2246.00	**0.049**	**0.034**

Notes: Abbreviations: eTIV, estimated total intracranial volume; FOG, freezing of gait; HC, healthy control; MMSE, mini-mental state examination; SiSt, sit to stand; PD, Parkinson's disease; 2nd, the second trial or return phase of the walking task. *r* represents Spearman's correlation coefficient. *P* values that less than 0.05 are given in bold.

We performed correlation and hierarchical clustering analysis across the 16 multimodal biomarkers (see Supplementary Figure S1), revealing several coherent structural relationships. Gait metrics formed a tightly interconnected cluster, exhibiting strong positive correlations (r ranges from 0.74 to 0.93, all $P<0.05$) among stride frequency and gait parameters, including walking step length, walking gait speed, straight walking-step length, and straight walking-gait speed. In contrast, turning left 360°-duration, turning 180°-duration, and freezing of gait (FOG)-longest duration showed moderate negative associations with this gait pace cluster (r ranges from −0.72 to −0.36, all $P<0.05$), reflecting the inverse relationship between dynamic stability and ambulation speed. Similarly, chair-stand performance metrics (chair stand-total duration and chair stand-mean duration) displayed moderate negative correlations with gait parameters (r ranges from −0.52 to −0.16, all $P<0.05$). Neuroimaging biomarkers organized into a distinct structural cluster with heterogeneous correlation patterns. Left cerebellum white matter and brain stem volume were moderately positively correlated ($r=0.31$, $P<0.05$). Neuroimaging biomarkers generally showed weak correlations with gait parameters in the global cohort ($|r|<0.30$, $P<0.05$), suggesting that regional neurodegeneration and motor performance may follow non-linear or subtype-specific trajectories. MMSE exhibited a unique correlational profile, showing moderate positive associations with walking gait speed and walking step

length (r ranges from 0.29 to 0.38, P<0.05) but limited linear correlation with neuroimaging biomarkers in the total cohort.

3.2 SuStaIn results

Cross-validation analysis identified a three-subtype model as the optimal solution, achieving the lowest CVIC=5215.48 among competing models (see Figure 2a). The model demonstrated robust stability, with a mean training log-likelihood of −874.84 and a mean test log-likelihood of −900.05. The close correspondence between training and test likelihoods confirms the model's generalizability and absence of overfitting. Furthermore, cluster discriminability was substantiated by a silhouette coefficient of 0.343 and a Calinski-Harabasz index of 27.88. These validity indices quantitatively confirmed that the identified subtypes were well-separated, with the silhouette coefficient measuring internal consistency and the Calinski-Harabasz index evaluating the ratio of inter-cluster to intra-cluster dispersion. The subtype classification demonstrated high reliability, achieving an average classification confidence score of 0.826. Based on the distinct profiles of these three subtypes, we designated them as gait-predominant, intermediate motor, and cognitive-predominant. Significant between-subtype differences were observed in SuStaIn disease staging (overall range: 0-12), with mean stages of 0.96 (gait-predominant), 2.42 (intermediate motor), and 4.67 (cognitive-predominant), respectively, see Figure 2b. In the training set, the three subtypes comprised the following distribution: n=48, 64.9% for gait-predominant subtype, n=19, 25.7% for intermediate motor subtype, and n=7, 9.4% for cognitive-predominant subtype, see Figure 2c.

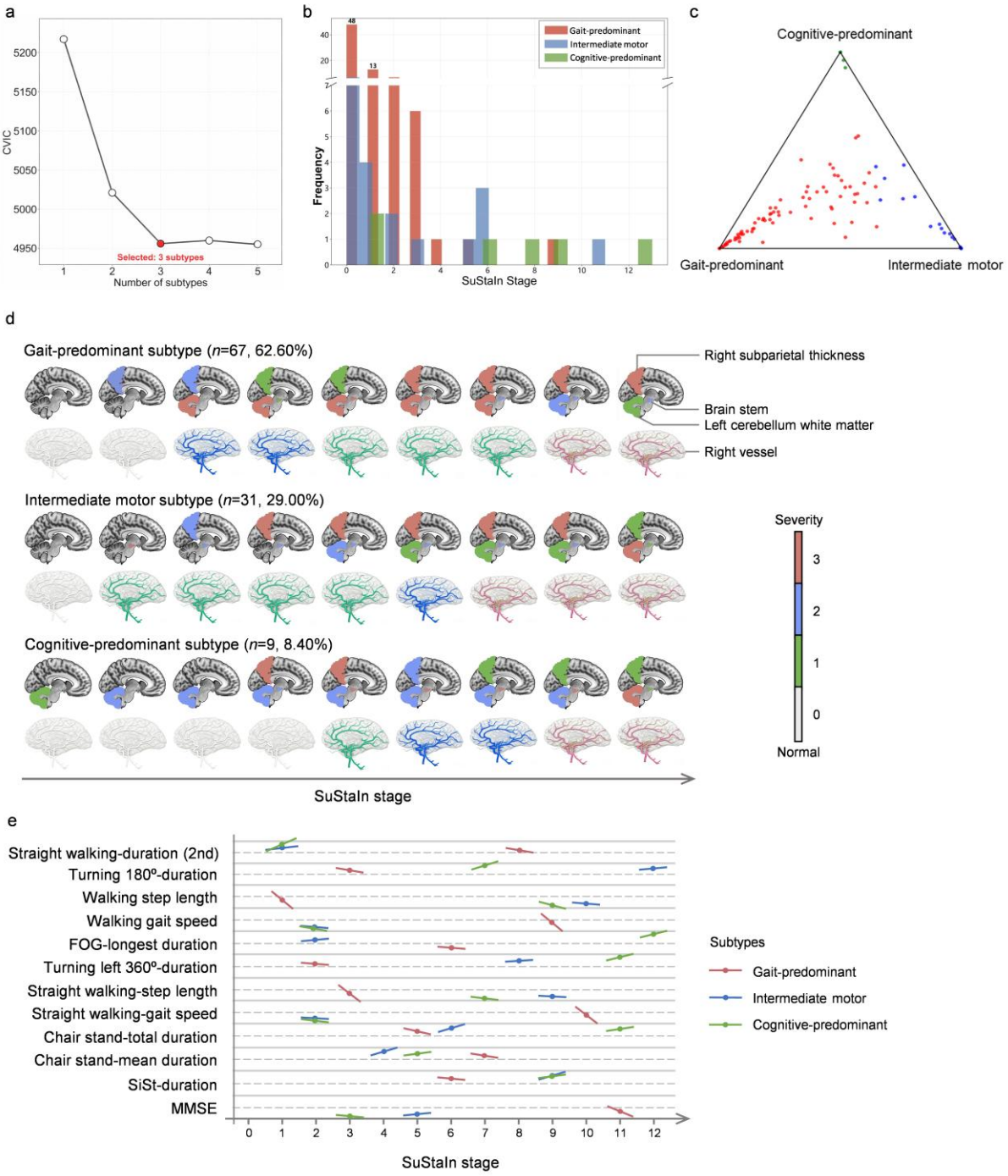


Figure 2 SuStaIn identified three subtypes of PD progression. (a) The number selection of subtypes based on CVIC across 10-fold cross-validation; (b) Stage distributions of participants across each subtype; (c) The certainty of subtype assignment for each participant, quantified as the maximum probability of belonging to the determined subtypes; (d) Regional brain atrophy progression patterns across the three subtypes; (e) The quantitative gait data and MMSE progression patterns with advancing disease stages across the three subtypes, where the dots represent the mean or median of the biomarkers in each specific subtypes, the position of the dots on the horizontal axis indicates the order in which the biomarkers exhibit abnormalities, the colored solid lines represent the trend of the biomarkers, while the dashed lines represent the mean value of HCs.

To evaluate the generalizability and robustness of the SuStaIn-derived subtypes, an independent test set comprising 33 PD patients was used for external validation. The distribution of subtypes in the test set (gait-

predominant subtype: *n*=19, 57.6%; intermediate motor subtype: *n*=12, 36.4%; cognitive-predominant subtype: *n*=2, 6.0%) closely resembled that of the training set. Chi-squared test validated that there existed no significant difference in subtype distribution between the two sets (χ^2=1.32, *P*=0.518), confirming stable and consistent subtype representation across the two datasets[34]. Furthermore, the Jensen-Shannon divergence (0.074) and Bhattacharyya coefficient (0.996) both suggested minimal distributional deviation and strong overlap between training and test sets, supporting the reproducibility of subtype assignment. Biomarker distribution analyses across the training and test sets further demonstrated consistent feature ranges, with global z-scores spanning from −3.69 to 6.89 in the training set and from −3.99 to 5.37 in the test set (see Supplementary Figure S2). All 16 gait, clinical, and neuroimaging biomarkers exhibited highly comparable density patterns between the two sets, validating the representative nature of the data partitioning. The maximum proportional difference in subtype composition was 8.04%, with a mean absolute difference of 5.36%, indicating negligible bias introduced during data partitioning. These findings validate the reliability of the model-derived subtypes and suggest that the multimodal SuStaIn framework maintains its discriminative power when applied to unseen data, reinforcing its potential for generalizable clinical translation.

3.3 Distinct biomarker progression trajectories

To comprehensively delineate the distinctions among the three subtypes, we integrated all PD cohort samples into the SuStaIn model, enabling visualization of the pseudo-trajectories of multimodal biomarkers across these subtypes (see Figure 2d-e). Six covariates and years of education were evaluated across the three SuStaIn-derived subtypes (see Table 2). None of these variables exhibited significant differences across the three subtypes (all *P*>0.05), indicating that subtype formation was not driven by demographic or anatomical differences.

The three subtypes displayed clearly differentiated temporal sequences of biomarker abnormalities. Events ordering in the gait-predominant subtype began with walking and turning performance, such as walking step length, turning left 360°-duration, straight walking-step length, turning 180°-duration, alongside initial thinning of the right subparietal cortex. Intermediate stages involved impairments in functional tasks, such as chair stand-total duration, FOG-longest duration, SiSt-duration, chair stand-mean duration, straight walking-duration (2nd), walking gait speed, straight walking-gait speed, and further structural alterations, including right vessel, left cerebellar white matter, and early brain stem involvement.

Notably, cognitive decline, as measured by MMSE, emerged primarily in the middle-to-later stages, indicating that this subtype is characterized by an early, selective deterioration in dynamic gait performance, with structural and cognitive changes emerging more gradually. The intermediate motor subtype exhibited a distinct temporal progression pattern characterized by sequential motor and structural abnormalities. Initial manifestations involved perturbations in speed and durations, such as straight walking-duration (2nd), walking gait speed, straight walking-gait speed. These were followed by impairments in functional mobility tasks, evidenced by increased durations for chair stand-mean duration, chair stand-total duration, SiSt-duration, turning left 360°-duration, alongside diminished straight walking-step length, walking step length, and turning 180°-duration. Notably, right vessel changes and brain stem alterations appeared earlier than the gait predominant subtype. Parietal thinning and turning impairments occurred in mid-sequence. Cognitive decline, as assessed by MMSE, became apparent during intermediate stages. Collectively, this subtype combined gait, lower-limb motor performance, and structural impairments from early progression. The cognitive-predominant subtype showed an initial sequence dominated by structural neuroimaging biomarkers, beginning with left cerebellum white matter changes, straight walking step length abnormalities, and turning impairment, followed by early MMSE decline and brain stem changes. Gait-speed abnormalities emerged later. This subtype presented the earliest cognitive involvement and the most advanced overall stages, with widespread multimodal abnormalities present by mid-trajectory. To visualize the temporal trends of multimodal biomarkers, we conducted a Spearman's correlation analysis between these biomarkers and the staging derived from SuStaIn, thereby delineating the approximate trajectory of each biomarker (see Figure 3 Progression trajectories of multimodal biomarkers by Spearman's correlation analysis with SuStaIn disease stage across the three subtypes. FOG, freezing of gait; MMSE, mini-mental state examination; SiSt, sit to stand. The symbols * and ** represent that *P* values are less than 0.05 and 0.01, respectively.). The results indicated that the majority of these biomarkers exhibited a progressive worsening trend correlating with disease staging. In summary, subtype-specific staging revealed a clear gradient of disease advancement. The gait-predominant subtype was primarily concentrated at the earliest stages, suggesting mild or nascent impairments. The intermediate motor subtype showed a more dispersed and progressive distribution, spanning from early to moderate stages. In contrast, the cognitive-predominant subtype occupied the most advanced stages, reflecting a more severe and widespread deterioration across multiple domains.

Averaged levels of the 16 multimodal biomarkers revealed significant variations across the three

subtypes, along with their correlations with disease stage (see Table 2 and Figure 3). Among the three subtypes, the gait-predominant subtype exhibited the lowest median values for both straight walking-duration (2nd) and turning 180°-duration, while demonstrating the highest mean values for walking step length, walking gait speed, straight walking-step length, and straight walking-gait speed. Notably, in the gait-predominant subtype, these six biomarkers were all significantly negatively correlated with disease stage (r=−0.357, r=−0.393, r=−0.777, r=−0.801, r=−0.715, r=−0.791, all P<0.01). In contrast, the cognitive-predominant subtype displayed significant positive correlations between straight walking-duration (2nd) and turning 180°-duration with disease stage (r = 0.939, r = 0.824, both P < 0.05). Furthermore, the intermediate motor subtype exhibited higher median values for chair stand-total duration, chair stand-mean duration, and SiSt-duration compared to the gait-predominant subtype, and all the three biomarkers showed significant positive correlations with disease stage (r=0.537, r=0.811, r=0.831, all P<0.01), whereas no such correlations were observed in the other two subtypes. The gait-predominant subtype also displayed the highest median MMSE score, which was significantly negatively correlated with disease stage (r = −0.310, P < 0.05), while no significant correlations were found for the other subtypes. No statistically significant differences were observed among the three subtypes for the four neuroimaging biomarkers. However, only the intermediate motor subtype exhibited a positive correlation between the right vessel marker and disease stage (r = 0.631, P < 0.01).

Moreover, the distribution of standardized MMSE scores (see Supplementary Figure S3) revealed subtype-specific cognitive profiles: the gait-predominant subtype exhibited relatively preserved cognition with a unimodal distribution centered above the standardized mean; the intermediate motor subtype showed a mild downward shift indicating early cognitive decline, whereas the cognitive-predominant subtype demonstrated a marked leftward skew suggestive of more severe impairment. Heatmap analysis of neuroimaging biomarkers (see Supplementary Figure S4) highlighted distinct regional patterns across subtypes. The cognitive-predominant subtype showed pronounced reductions in left cerebellum white matter and right vessel volume, whereas the intermediate motor subtype demonstrated relatively lower brain stem volume but increased right vessel volume and subparietal thickness.

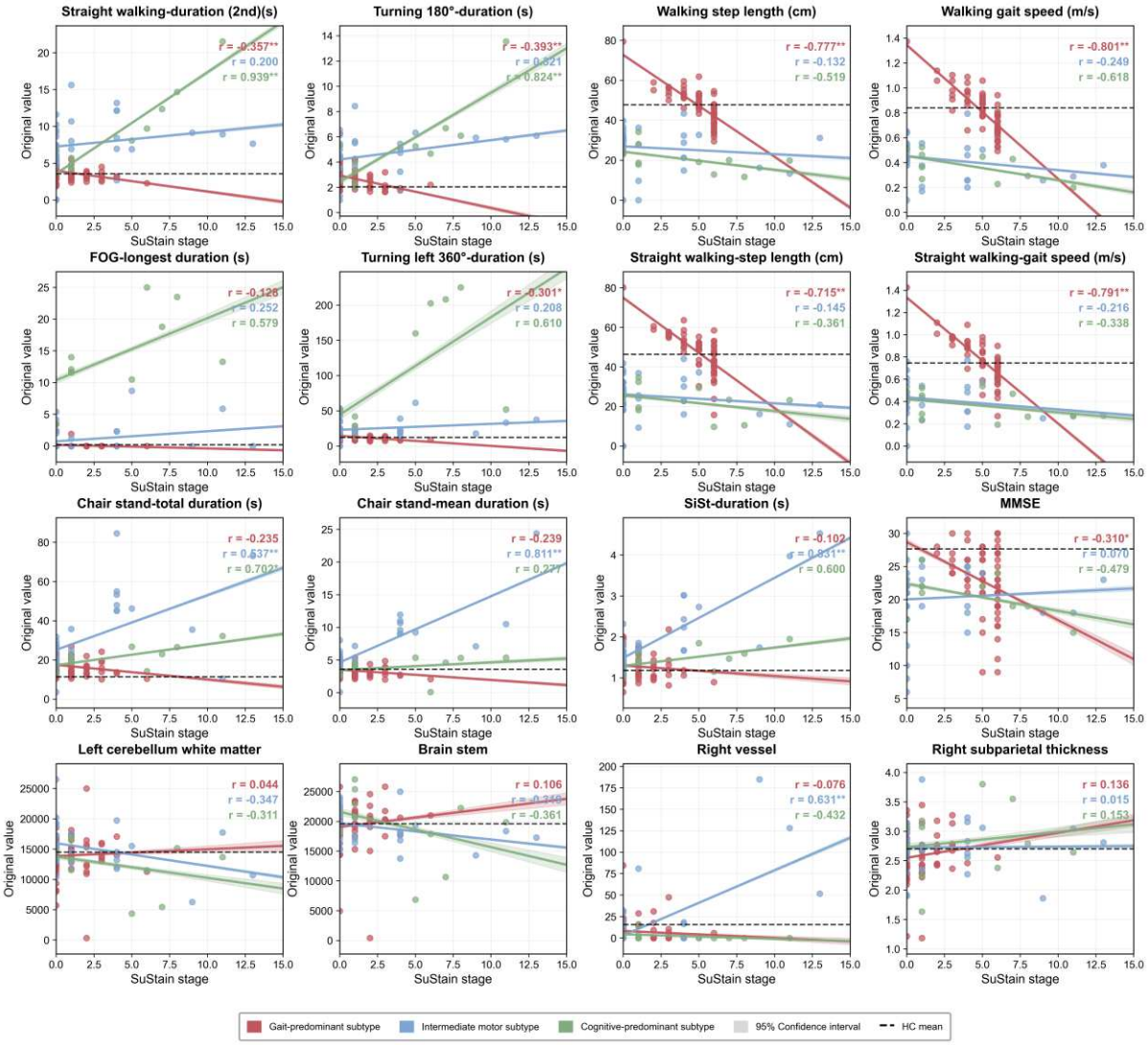


Figure 3 Progression trajectories of multimodal biomarkers by Spearman's correlation analysis with SuStaIn disease stage across the three subtypes. FOG, freezing of gait; MMSE, mini-mental state examination; SiSt, sit to stand. The symbols * and ** represent that *P* values are less than 0.05 and 0.01, respectively.

Table 2 Differences of multimodal biomarker profiles among the three SuStaIn-derived PD subtypes

Characteristics	Gait-predominant (*n* = 67; 62.6%)	Intermediate motor (*n* = 31; 29.0%)	Cognitive-predominant (*n* = 9; 8.4%)	*P*
Gender (Male/Female)	40/27	15/16	5/4	0.576
Age	66.30±9.70	71.10±5.80	71.70±7.70	0.072
Height (cm)	165.00 [160.00, 170.00]	160.00 [155.00, 170.00]	165.50 [156.20, 172.80]	0.523
Thigh length (cm)	45.00 [42.00, 46.00]	43.00 [40.00, 46.20]	41.00 [40.00, 41.80]	0.102
Calf length (cm)	44.00 [42.00, 45.00]	42.00 [40.00, 45.0]	42.50 [40.20, 43.80]	0.189
eTIV	1353089.70 [1222198.10, 1424868.30]	1284119.20 [1179564.60, 1453009.10]	1448340.30 [1257141.60, 1647060.70]	0.601
Years of education	7.59±4.15	6.88±4.04	7.50±3.55	0.728
Straight walking-duration (2nd)(s)	3.41 [2.95, 4.49]	7.46 [6.00, 9.28] [a]	7.58 [5.05, 11.70] [a]	**<0.001**
Turning 180°-duration (s)	2.49 [2.02, 3.09]	4.65 [3.55, 5.55] [a]	4.97 [3.46, 5.90] [a]	**<0.001**

Walking step length (cm)	46.32±10.05	27.02±10.21[a]	16.87±3.63[a,b]	**<0.001**
Walking gait speed (m/s)	0.80±0.20	0.42±0.15[a]	0.30±0.09[a,b]	**<0.001**
FOG-longest duration (s)	0.08±0.48	0.42 ± 0.15[a]	17.40±5.90[a,b]	**<0.001**
Turning left 360°-duration (s)	11.89 [9.31, 14.39]	22.43 [17.38, 33.57] [a]	51.66 [32.09, 192.03] [a,b]	**<0.001**
Straight walking-step length (cm)	47.17±10.07	25.21±10.71 [a]	22.36±8.36 [a]	**<0.001**
Straight walking-gait speed (m/s)	0.77±0.18	0.42±0.17 [a]	0.37±0.13 [a]	**<0.001**
Chair stand-total duration (s)	16.09 [13.48, 19.50]	26.16 [20.08, 38.15] [a]	21.62 [18.45, 25.71] [a]	**<0.001**
Chair stand-mean duration (s)	3.20 [2.66, 4.17]	5.42 [4.13, 9.03][a]	4.47 [4.32, 5.14]	**<0.001**
SiSt-duration (s)	1.22 [1.05, 1.45]	1.67 [1.38, 1.96] [a]	1.45 [1.34, 1.59] [a]	**<0.001**
MMSE	23.00 [21.00, 27.00]	21.00 [18.00, 24.00] [a]	21.50 [19.00, 22.00] [a]	**0.005**
Left cerebellum white matter	14036.80 [12426.90, 15830.90]	14534.05 [13209.95, 17386.25]	13497.55 [11543.83, 15086.90]	0.692
Brain stem	19853.92±2318.24	18279.06±2922.69	19716.33±5408.29	0.083
Right vessel	2.35 [0.00, 15.15]	1.50 [0.00, 19.25]	0.00 [0.00, 2.25]	0.269
Right subparietal thickness	2.57 [2.38, 2.78]	2.73 [2.55, 3.00]	2.93 [2.45, 3.15]	0.577

Notes: The symbols a and b represent that there exist significant differences compared to the gait-predominant subtype and the intermediate motor subtype, respectively. *P* values that less than 0.05 are given in bold.

To facilitate domain-level analysis, gait-related biomarkers were categorized into six composite domains: walking duration (straight walking-duration (2nd), turning 180°-duration, SiSt-duration), step length (walking step length, straight walking-step length), gait speed (walking gait speed, straight walking-gait speed), turning duration (turning left 360°-duration), chair stand (chair stand-total duration, chair stand-mean duration), and persistent characteristics (FOG-longest duration), with standardized scores computed for inter-subtype comparison (see Figure 4a). Gait metrics differed markedly across the three SuStaIn-derived subtypes. Gait-predominant subtype showed the lowest median values of walking duration, turning duration, chair stand, and persistent characteristics, and the highest median values of step length and gait speed, indicating relatively preserved pace, step length and speed. Cognitive-predominant subtype exhibited the most pronounced impairments by the lowest median values of step length, and the highest medians of turning duration and persistent characteristics, indicating severe and sustained disruption of continuous locomotion and turning control. Intermediate motor subtype presented intermediate gait performance across the six domains, consistent with combined impairments in pace and lower-limb strength.

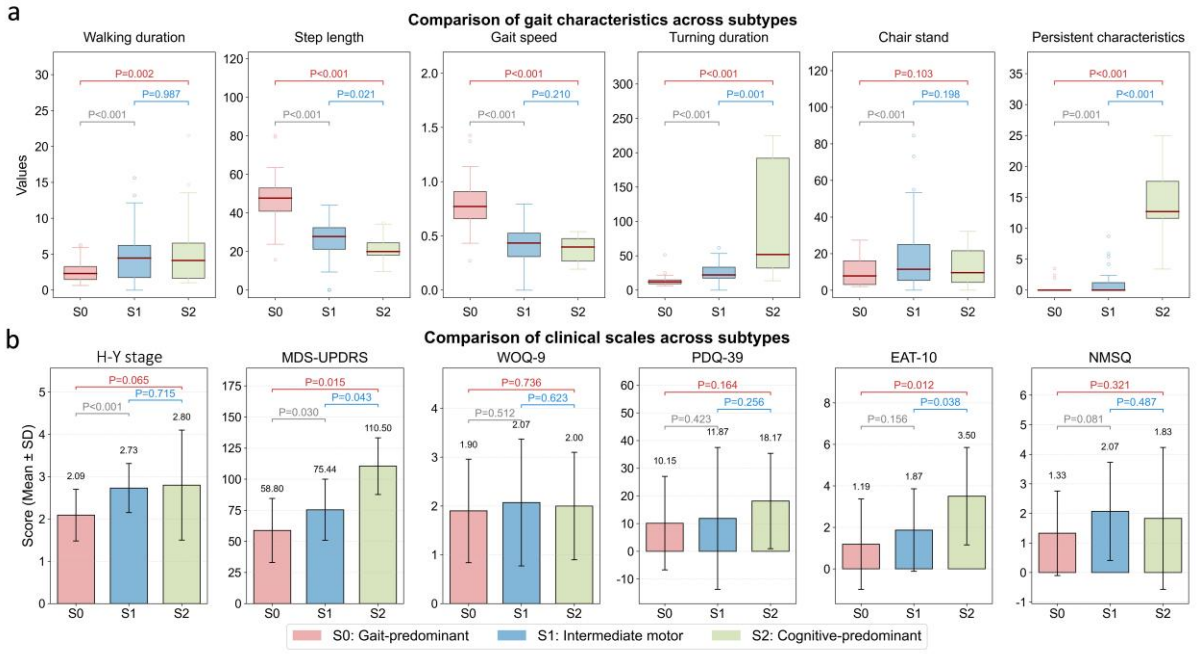


Figure 4 Multimodal gait metrics and clinical profiles exhibited differences across the three SuStaIn-derived PD subtypes. (a) The box plots for comparison results of gait characteristics across the three subtypes; (b) The error bar plots for comparison results of clinical scales across the three subtypes.

3.4 Subtype-specific differences in clinical outcomes

The cognitive-predominant subtype exhibited a "malignant" clinical profile characterized by the highest disease burden (see Figure 4b). The MDS-UPDRS for this group was nearly twofold that of the gait-predominant subtype, while the intermediate motor subtype exhibited intermediate values. Similarly, H-Y staging confirmed a severity gradient: the gait-predominant subtype clustered at a milder stage, whereas both the intermediate motor and cognitive-predominant subtypes exhibited more advanced progression. Critically, the cognitive-predominant subtype was the only group to show clinically significant signs of bulbar dysfunction, corroborating the brain stem atrophy observed on MRI. The EAT-10 scores in this group exceeded the clinical cutoff for dysphagia risk ($\geqslant 3$), significantly higher than the other two subtypes. Although trends indicated poorer quality of life (PDQ-39) in the cognitive-predominant subtype (mean=18.17vs.10.35 in gait-predominant) and slightly higher non-motor burden (NMSQ), these differences did not reach statistical significance ($P>0.05$), likely due to the limited sample size of the severe subtype. No significant differences were observed in the wearing-off phenomenon (WOQ-9).

Moreover, correlation analysis revealed no significant linear relationship between the data-driven SuStaIn stages and the ordinal H-Y stages across the PD cohort and within individual subtypes (see Supplementary Figure S5). This dissociation suggests that SuStaIn captures granular biological progression

that occurs within the broad categorical steps of the H-Y scale.

4 Discussion

In this study, we leveraged the data-driven SuStaIn framework to unravel the spatiotemporal heterogeneity of PD from multimodal biomarkers. By integrating wearable sensor-based gait metrics, clinical assessments, and structural neuroimaging, we identified three robust subtypes—gait-predominant, intermediate motor, and cognitive-predominant—each defined by a unique chronological sequence of biomarker abnormalities. These trajectories provide biologically grounded insights into the diverse pathological mechanisms underlying PD progression.

The gait-predominant subtype recapitulates the canonical motor progression of PD. The earliest events in this trajectory involved selective deficits in gait speed and step length, markers closely linked to the progressive degeneration of the nigrostriatal dopaminergic pathway[1,35]. Crucially, this subtype exhibited a sequential pattern where non-dopaminergic features such as significant cognitive decline, postural instability, and widespread structural atrophy, emerged only as late, secondary phenomena. This temporal ordering suggests that the gait-predominant subtype represents a pure dopaminergic phenotype in its early phases, where pathology is initially confined to the substantia nigra before slowly spreading to extranigral regions. This aligns with the "slow-progression" motor-dominant phenotypes described in longitudinal cohorts[3]. In stark contrast, the intermediate motor subtype displayed an "axial-malignant" signature, characterized by the concurrent early impairment of gait pace and dynamic stability (e.g., turning duration, chair-stand performance). While clinically resembling the postural instability and gait difficulty phenotype[36], our model refines the mechanistic understanding of this group. Turning and postural control are heavily reliant on the cholinergic system, particularly the pedunculopontine nucleus in the brainstem and its projections to the thalamus and basal forebrain[37]. The early involvement of these axial metrics in the mixed motor trajectory likely reflects cholinergic dysfunction occurring concurrently with, rather than secondary to, dopaminergic loss. Thus, this subtype should be viewed as a manifestation of early multi-system neurotransmitter failure, explaining its association with rapid progression and elevated fall risk[37].

A novel and pivotal finding of our study is the identification of the cerebellum's distinct temporal role in the cognitive-predominant subtype. Our data demonstrated that significant cerebellar white matter atrophy represents an early defining event in this group, preceding its manifestation in the gait-predominant trajectory. This challenges the conventional paradigm of the cerebellum as merely a motor coordinator in PD. These

findings suggest that the rapid cognitive decline observed in this subtype may result from structural disintegration of the cerebello-thalamo-cortical circuit. Modern neuroanatomical frameworks established that the cerebellum modulates executive function and cognition through reciprocal loops with the prefrontal and parietal cortices[38,39]. Importantly, this rapid cognitive decline is likely driven by specific network pathology rather than lower baseline cognitive reserve, as years of education were comparable across all subtypes. In the gait-predominant subtype, cerebellar integrity was preserved until late stages, consistent with the hypothesis that the cerebellum acts as a compensatory driver to maintain function in the face of basal ganglia dysfunction[38]. However, in the cognitive-predominant subtype, the premature degeneration of cerebellar white matter signifies a failure of this compensatory mechanism. This structural disconnection may lead to "dysmetria of thought"—a disruption in the universal cerebellar transform applied to cognitive processing, as previous study termed[40]. Crucially, the structural brainstem atrophy detected by our model is functionally corroborated by independent clinical validation. The cognitive-predominant subtype was the only group to exhibit significant bulbar dysfunction (elevated EAT-10 scores). Since the swallowing reflex is mediated by the brainstem reticular formation, this clinical-radiological concordance strongly supports the presence of genuine, high-load pathology in the posterior fossa. Consequently, the "cognitive-motor" dual decline in this subtype represents a specific network vulnerability, where the breakdown of long-range connectivity accelerates clinical deterioration.

The identification of these multimodal trajectories prompts a re-evaluation of PD pathological progression models. The cognitive-predominant subtype shares features with the proposed "brain-first" hypothesis, which posits that α-synuclein pathology may originate intracranially and spread to cortical areas, leading to cognitive deficits before severe motor signs[41]. However, a nuanced interpretation is required. The prominent and concurrent involvement of the brainstem and cerebellum in our model suggests that this is not simply a "top-down" cortical disease, but rather a "diffuse malignant" phenotype characterized by an aggressive and widespread α-synuclein load [3]. Although our study did not incorporate specific biomarkers for prodromal staging, such as RBD or MIBG scintigraphy, the observed trajectory demonstrates that structural atrophy in the posterior fossa coincides with rapid cognitive decline. This pattern aligns with a pathological mechanism characterized by rapid dissemination across multiple synaptic pathways. Whether this theoretically represents a "brain-first" origin with rapid descending spread, or an aggressive "body-first" pathology with accelerated ascending velocity, the outcome is a high-pathology load state[41]. This

characterization of a “malignant” phenotype is further substantiated by the MDS-UPDRS, which was nearly double that of the gait-predominant group. Such a disproportionate global burden reflects a pervasive collapse of motor and non-motor systems, emphasizing the need for early stratification, as these patients may require therapeutic strategies targeting non-dopaminergic pathways and neuroprotection rather than symptomatic motor control alone.

Several limitations of the present study should be acknowledged. First, the sample size of the cohort, especially the cognitive-predominant subtype, was relatively small, potentially limiting the generalizability of the findings, despite robust performance demonstrated through cross-validation and external testing. Second, while the cross-sectional design was appropriate for SuStaIn modeling, it cannot substitute for longitudinal validation. Future studies incorporating longitudinal follow-up would enhance the refinement of subtype trajectories and facilitate the prediction of individual subtype transitions. Finally, the cohort was recruited from a single clinical center, and multi-site validation would strengthen the external generalizability of the results.

5 Conclusion

By integrating wearable sensor-based gait metrics, clinical assessments, and neuroimaging biomarkers, our study uncovered three biologically coherent subtypes with distinct spatiotemporal trajectories: a frequent gait-predominant phenotype reflecting canonical, slow-progressing dopaminergic degeneration; an intermediate motor phenotype characterized by concurrent axial and appendicular dysfunction; and a malignant cognitive-predominant phenotype driven by premature cerebellar and brainstem atrophy. These subtype-specific trajectories align closely with mechanistic evidence from neuropathology, offering a robust framework for precision medicine. By enabling the inference of longitudinal disease dynamics from cross-sectional data, our approach facilitates individualized prognostic prediction and biomarker-guided stratification, which are critical for enriching clinical trials and developing targeted neuroprotective therapies.

List of abbreviations

CVIC: Cross-validation information criterion

EAT-10: Eating assessment too

eTIV: estimated total intracranial volume

FOG: Freezing of gait

HC: Healthy control

H-Y: Hoehn & Yahr

IMU: Inertial measurement unit

MDS-UPDRS: Movement Disorder Society-Unified Parkinson's disease rating scale

MMSE: Mini-mental state examination

MRI: Magnetic resonance imaging

NMSQ: Non-motor symptoms questionnaire

PD: Parkinson's disease

PDQ-39: 39-item PD questionnaire

SiSt: Sit to stand

SuStaIn: Subtype and stage inference

WOQ-9: Wearing-off questionnaire

Acknowledgements

The authors want to express our gratitude to the patients and their families.

Author contributions

ZL and LX: Formal analysis, writing-review & editing, and visualization. YL, DC, CL, AG and HY: Resources and investigation. PL and HB: Writing-original draft. LR and LX: Supervision and project administration. PL: Data curation and software. LX: Conceptualization and methodology.

Consent to participates

All participants gave their informed permission in this study.

Declaration of conflicting interest

All authors declare no financial or non-financial competing interests.

Funding statement

This study was funded by the Open Project of Jiangsu Provincial Key Laboratory (Grant No. XZSYSKF2023.28), the Xuzhou Science and Technology Bureau Project (Grant No. KC23155), and the Affiliated Hospital of Xuzhou Medical University Research Fund (Grant No. XYF202249). The funder played no role in study design, data collection, analysis and interpretation of data, or the writing of this manuscript.

Data availability

The datasets analyzed during the current study are available from the corresponding author on reasonable request.

Code availability

The code for SuStaIn model construction (https://github.com/ucl-pond/pySuStaIn) are open sources.

Supplemental materials

Supplementary materials include: Supplementary methods; Supplementary tables and figures: Table S1 Candidate multimodal indicators in healthy controls and patients with Parkinson's disease in the training set; Figure S1 Correlation matrix and hierarchical clustering of the selected multimodal biomarkers; Figure S2 Consistent biomarker distributions between training and test sets; Figure S3 Distribution of standardized MMSE scores across SuStaIn-derived subtypes; Figure S4 Heatmap of mean standardized neuroimaging biomarkers across SuStaIn-derived subtypes; Figure S5 Correlation analysis between data-driven SuStaIn stages and clinical Hoehn & Yahr (H-Y) staging.

References

1. Kalia, L. V. & Lang, A. E. Parkinson's disease. *Lancet* **386**, 896–912 (2015).
2. Hayes, M. T. Parkinson's disease and Parkinsonism. *The American Journal of Medicine* **132**, 802–807 (2019).
3. Fereshtehnejad, S.-M., Zeighami, Y., Dagher, A. & Postuma, R. B. Clinical criteria for subtyping Parkinson's disease: biomarkers and longitudinal progression. *Brain* **140**, 1959–1976 (2017).
4. Mestre, T. A. *et al.* Parkinson's Disease Subtypes: Critical Appraisal and Recommendations. *J Parkinsons Dis* **11**, 395–404 (2021).
5. Lawton, M. *et al.* Developing and validating Parkinson's disease subtypes and their motor and cognitive progression. *J Neurol Neurosurg Psychiatry* **89**, 1279–1287 (2018).
6. Pourzinal, D. *et al.* Identifying subtypes of mild cognitive impairment in Parkinson's disease using cluster analysis. *J Neurol* **267**, 3213–3222 (2020).
7. Totsune, T. *et al.* Nuclear imaging data-driven classification of Parkinson's disease. *Mov Disord* **38**, 2053–2063 (2023).
8. Zhang, Z. *et al.* Identification of depression subtypes in Parkinson's disease patients via structural MRI whole-brain radiomics: An unsupervised machine learning study. *CNS Neurosci Ther* **31**, e70182 (2025).
9. Fereshtehnejad, S.-M., Zeighami, Y., Dagher, A. & Postuma, R. B. Clinical criteria for subtyping Parkinson's disease: Biomarkers and longitudinal progression. *Brain* **140**, 1959–1976 (2017).
10. Albrecht, F. *et al.* Unraveling Parkinson's disease heterogeneity using subtypes based on multimodal data. *Parkinsonism Relat Disord* **102**, 19–29 (2022).
11. Latourelle, J. C. *et al.* Large-scale identification of clinical and genetic predictors of motor progression in patients with newly diagnosed Parkinson's disease: a longitudinal cohort study and validation. *Lancet Neurol* **16**, 908–916 (2017).
12. Fereshtehnejad, S.-M., Zeighami, Y., Dagher, A. & Postuma, R. B. Clinical criteria for subtyping Parkinson's disease: biomarkers and longitudinal progression. *Brain* **140**, 1959–1976 (2017).
13. Del Din, S., Godfrey, A., Mazzà, C., Lord, S. & Rochester, L. Free-living monitoring of Parkinson's disease: Lessons from the field. *Mov Disord* **31**, 1293–1313 (2016).
14. Teague, S. *et al.* Retention strategies in longitudinal cohort studies: a systematic review and meta-analysis. *BMC Med Res Methodol* **18**, 151 (2018).
15. Mirelman, A. *et al.* Gait impairments in Parkinson's disease. *Lancet Neurol* **18**, 697–708 (2019).
16. Oxtoby, N. P., Alexander, D. C., & EuroPOND consortium. Imaging plus X: multimodal models of neurodegenerative disease. *Curr Opin Neurol* **30**, 371–379 (2017).
17. Fonteijn, H. M. *et al.* An event-based model for disease progression and its application in familial Alzheimer's disease

and Huntington's disease. *Neuroimage* **60**, 1880–1889 (2012).

18. Venkatraghavan, V., Bron, E. E., Niessen, W. J., Klein, S., & Alzheimer's Disease Neuroimaging Initiative. Disease progression timeline estimation for Alzheimer's disease using discriminative event based modeling. *Neuroimage* **186**, 518–532 (2019).
19. Young, A. L. *et al.* Uncovering the heterogeneity and temporal complexity of neurodegenerative diseases with Subtype and Stage Inference. *Nat Commun* **9**, 4273 (2018).
20. Aksman, L. M. *et al.* pySuStaIn: a Python implementation of the Subtype and Stage Inference algorithm. *SoftwareX* **16**, 100811 (2021).
21. Thung, K.-H., Wee, C.-Y., Yap, P.-T., Shen, D., & Alzheimer's Disease Neuroimaging Initiative. Neurodegenerative disease diagnosis using incomplete multi-modality data via matrix shrinkage and completion. *Neuroimage* **91**, 386–400 (2014).
22. Young, A. L. *et al.* Ordinal SuStaIn: Subtype and Stage Inference for Clinical Scores, Visual Ratings, and Other Ordinal Data. *Front Artif Intell* **4**, 613261 (2021).
23. Postuma, R. B. *et al.* MDS clinical diagnostic criteria for Parkinson's disease. *Mov Disord* **30**, 1591–1601 (2015).
24. Fischl, B. FreeSurfer. *Neuroimage* **62**, 774–781 (2012).
25. Sowell, E. R. *et al.* Longitudinal mapping of cortical thickness and brain growth in normal children. *J Neurosci* **24**, 8223–8231 (2004).
26. Del Din, S., Godfrey, A., Mazzà, C., Lord, S. & Rochester, L. Free-living monitoring of Parkinson's disease: Lessons from the field. *Mov Disord* **31**, 1293–1313 (2016).
27. Weiss, A. *et al.* Can an accelerometer enhance the utility of the Timed Up & Go Test when evaluating patients with Parkinson's disease? *Med Eng Phys* **32**, 119–125 (2010).
28. Young, A. L. *et al.* Uncovering the heterogeneity and temporal complexity of neurodegenerative diseases with Subtype and Stage Inference. *Nat Commun* **9**, 4273 (2018).
29. Young, A. L. *et al.* A data-driven model of biomarker changes in sporadic Alzheimer's disease. *Brain* **137**, 2564–2577 (2014).
30. Eshaghi, A. *et al.* Identifying multiple sclerosis subtypes using unsupervised machine learning and MRI data. *Nat Commun* **12**, 2078 (2021).
31. La Joie, R. *et al.* Region-specific hierarchy between atrophy, hypometabolism, and β-amyloid (Aβ) load in Alzheimer's disease dementia. *J. Neurosci.* **32**, 16265–16273 (2012).
32. Eshaghi, A. *et al.* Identifying multiple sclerosis subtypes using unsupervised machine learning and MRI data. *Nat*

Commun **12**, 2078 (2021).

33. Oxtoby, N. P. *et al.* Data-driven models of dominantly-inherited Alzheimer's disease progression. *Brain* **141**, 1529–1544 (2018).
34. Hely, M. A., Reid, W. G. J., Adena, M. A., Halliday, G. M. & Morris, J. G. L. The Sydney multicenter study of Parkinson's disease: the inevitability of dementia at 20 years. *Mov Disord* **23**, 837–844 (2008).
35. Mirelman, A. *et al.* Gait impairments in Parkinson's disease. *Lancet Neurol* **18**, 697–708 (2019).
36. Stebbins, G. T. *et al.* How to identify tremor dominant and postural instability/gait difficulty groups with the movement disorder society unified Parkinson's disease rating scale: comparison with the unified Parkinson's disease rating scale. *Mov Disord* **28**, 668–670 (2013).
37. Bohnen, N. I. & Albin, R. L. The cholinergic system and Parkinson disease. *Behav Brain Res* **221**, 564–573 (2011).
38. Wu, T. & Hallett, M. The cerebellum in Parkinson's disease. *Brain* **136**, 696–709 (2013).
39. Middleton, F. A. & Strick, P. L. Anatomical evidence for cerebellar and basal ganglia involvement in higher cognitive function. *Science* **266**, 458–461 (1994).
40. Schmahmann, J. D. & Sherman, J. C. The cerebellar cognitive affective syndrome. *Brain* **121 (Pt 4)**, 561–579 (1998).
41. Horsager, J. *et al.* Brain-first versus body-first Parkinson's disease: a multimodal imaging case-control study. *Brain* **143**, 3077–3088 (2020).

Supplementary Files

This is a list of supplementary files associated with this preprint. Click to download.

- SupplementaryMaterials.docx